The International Journal of Advanced Manufacturing Technology (2018) 95:4153–4162
https://doi.org/10.1007/s00170-017-1358-y

ORIGINAL ARTICLE

Prediction of distortion induced by machining residual stresses in thin-walled components

Junteng Wang[1] · Dinghua Zhang[1] · Baohai Wu[1] · Ming Luo[1]

Received: 23 May 2017 / Accepted: 9 November 2017 / Published online: 5 January 2018
© Springer-Verlag London Ltd., part of Springer Nature 2018

Abstract
Machining of thin-walled components is standard practice in many fields such as spaceflight, aviation, automobile, medical equipment manufacturing, etc. When these thin-walled components are machined, however, part distortions arise from machining-induced stresses resulting from high cutting forces and temperatures. In this paper, a method of predicting distortion induced by machining residual stresses in thin-walled components is proposed, which includes an empirical model for predicting machining residual stresses with different cutting parameters and a modified FEM model for predicting the resulted distortion. On the basis of the measured residual stress results, an exponentially decaying sine function is fitted using the particle swarm optimization method and the coefficients of the fitting function are regressed with cutting parameters. General FEM software ABAQUS is used to create and mesh the thin-walled component. Standard parts of the same material with the experimental samples are machined to make modification to the predicted residual stress profiles under the arranged cutting conditions. The modified residual stress distributions are applied into ABAQUS to calculate the distortion of the experimental samples. Two experimental samples are machined to validate the prediction methodology. The results demonstrate that the proposed method can significantly improve the distortion prediction accuracy.

Keywords Distortion · Residual stresses · Empirical model · Modification · Thin-walled components

1 Introduction

Thin-walled components made of alloys with a high strength to weight ratio are widely used in the fields such as spaceflight, aviation, automobile, medical equipment manufacturing, etc. Part distortion induced by residual stresses, which leads to an increase in the failure rate of components and the cost of production, is a serious manufacturing challenge in machining of these thin-walled components. According to a report by Boeing, in some thin walled parts, the probability that the distortion causes a part to miss the engineering tolerances is 47%. The estimated costs of rework and scrap due only to distortion after machining costs manufacturers 10 million dollars annually [1]. One main source of these distortions of components was the distortion induced by residual stresses.

Residual stresses are stresses that remain in components after the original cause of the stresses has been removed. In general, residual stresses in machining can be classified into two types. The first one, bulk residual stresses, refers to the stresses induced by various processes such as melting of alloys, rolling and quenching during the material manufacturing. The second one, machining induced residual stresses, refers to the stresses introduced due to the thermo-mechanical behavior of the cutting process during the machining process [2]. Machining-induced residual stresses were reported to be greatly affected by cutting parameters [3–6].

Both these types of residual stresses can lead to significant dimensional instability through distortion. In machining, the equilibrium state of bulk residual stresses was broken with materials removal, the bulk stresses redistributed with the distortion of parts. On the other hand, machining residual stresses were induced in the near surface layer due to the high mechanical and thermal loads in the machining processes, which may cause an imbalance in internal stresses. Hence, new distortion occurred to balance these residual stresses. Researchers have tried to find the main influence factors of the machining distortion induced by residual stresses. Huang [7] investigated the principal factors influencing the monolithic component

✉ Baohai Wu
wubaohai@nwpu.edu.cn

[1] Key Laboratory of Contemporary Design and Integrated Manufacturing Technology, Northwestern Polytechnical University, Ministry of Education, Xi'an 710072, China

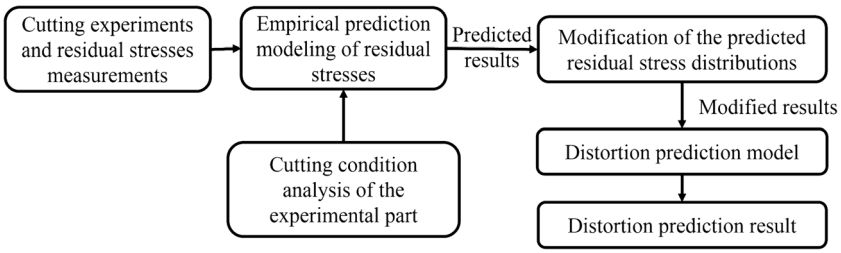

Fig. 1 The concrete realization steps of the proposed method

deformation by finite element simulation and experiment. The research pointed out that the bulk residual stress in the blank dominated the deformation of three-frame monolithic beam since the deformation caused by the blank initial residual stress accounted for 90% of the total deformation. Yang [8] showed that the initial residual stress in the blank is the major influence factor of machining distortion for aluminum alloy aircraft monolithic component. However, Young [9] pointed out that the effect of machining-induced residual stresses on distortion tends to increase with decreasing thickness. The machining-induced stress can be a dominant effect when thin-walled parts are finish machined. Particularly, thin-walled components with great lateral dimensions can exhibit significant shape deviations because of machining-induced residual stress.

Prediction of machining induced distortion has been studied by many researchers. FEM models are the main research means. Marusich [10] developed a FEM software to predict and control distortions of components. Both the bulk residual stresses and the machining induced residual stresses were taken into account. A simplified shell model of the workpiece was used to calculate the distortion of the machined workpiece. Zhang [11] minimized the machining distortion of T-shaped components by investigating the influence of material removal partition on residual stress. The results showed that part distortion is mainly affected by the partition of material removal in T-shaped components. Brinksmeier [12] predicted the shape deviation of machined components with complex geometry by combining experimental data with simple geometries and FEM simulations. Cerutti [13] developed a specific finite element tool to predict the behavior of the workpiece during machining due to its changing geometry and fixture-workpiece contacts. This numerical tool utilized a material removal approach which enables it to simulate the machining of parts with complex geometries. Moreover, Cerutti [14] further used this specific numerical tool to study the influence of the machining sequence on the machining distortion with the initial residual stresses taken into consideration. Analytical method and experimental method were also adopted by some researchers. Fergani [15] developed an analytical model for predicting the residual stresses induced by the milling process and the post machining distortion of the machined thin plate. Prediction results of the analytical model for a final thin plate presented an acceptable agreement with experiment. The maximum registered error was less than 30%. Masoudi [16] investigated the correlation between machining induced residual stresses and distortion in a thin-walled cylinder experimentally. The results indicated that the force and temperature have direct effects on the residual stresses and distortion in the thin-walled parts. Most of these studies did not clearly distinguish the roughing stage and finishing stage of the machining process. Most of these research efforts have focused on the

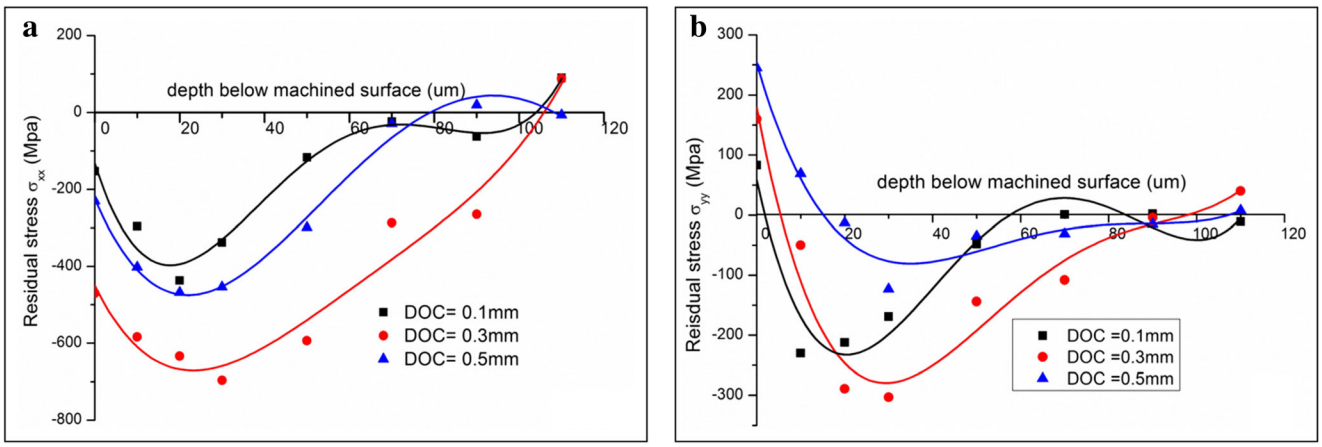

Fig. 2 Residual stress profiles for different DOC (depth of cut), (a)σ_{xx}, (b)σ_{yy}, (width of cut 0.2 mm, cutting speed 60 m/min, federate 0.06 mm/rev, lead angle 10°, tilt angle 0°, with cooling) [20]

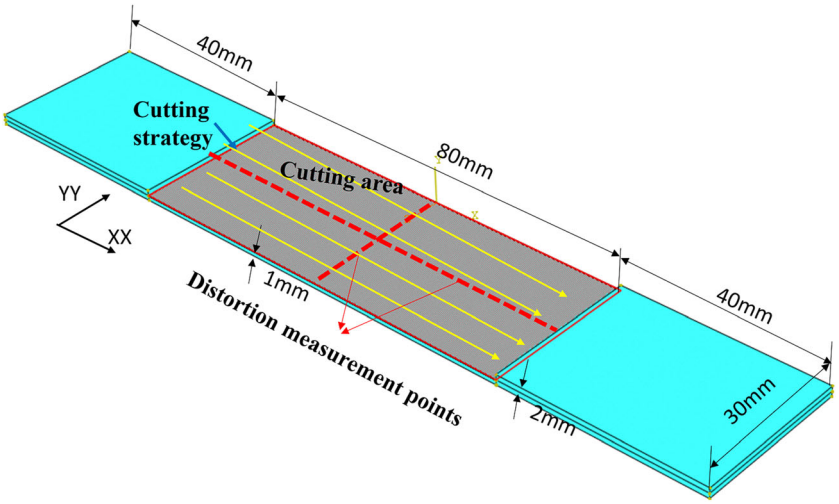

Fig. 3 Details of the standard part

distortion induced by the re-equilibrium of bulk stresses. The blank used by these researchers usually were thick plates and most of the materials were removed during the roughing stage of machining. However, in the machining of thin-walled components, especially components used in the aerospace applications, stress relief treatment process and contour modification process were usually applied after the roughing stage to eliminate the influence of bulk stresses. In the finishing stage of the machining process, the parts were thin enough that the dominant factor for distortion of these thin-walled components was the machining induced residual stresses. Machining-induced stresses acted as the main source of distortion and dimensional instability. Thus, in this paper, the research efforts are focused on the machining induced residual stresses and the resulted distortion of thin walled components. In the previous studies, researchers tended to apply the predicted or measured machining induced residual stresses on the near surface layer of the workpieces to calculate the final distortions. However, it is very difficult to obtain accurate values of the residual stresses induced by machining. The inaccurate residual stress distributions caused a negligible error in the prediction of distortion. Therefore, further efforts are needed to predict the distortion induced by machining residual stresses more accurately.

In this paper, a method of predicting distortion induced by machining residual stresses is proposed. The distortion can be predicted based on cutting conditions. An empirical model for prediction of machining-induced residual stresses is established with the cutting parameters as the input data. The predicted machining-induced residual stress distributions are modified by the machining of standard parts. Then, the distortions of two experimental samples were predicted using FEM model with the modified residual stresses as the input data. Finally, experiments are conducted to validate the prediction methodology.

Table 1 Distortions of the standard part

$\overline{\sigma}_{xx}$ (MPa)	$\overline{\sigma}_{yy}$ (MPa)	δ_{xx}(mm)	δ_{yy}(mm)
−250	−250	1.27	1.33E-01
−250	−150	1.4	5.77E-02
−250	−50	1.54	−1.79E-02
−150	−250	6.23E-01	1.55E-01
−150	−150	7.59E-01	7.99E-02
−150	−50	8.96E-01	4.39E-03
−50	−250	−1.97E-02	1.78E-01
−50	−150	1.17E-01	1.02E-01
−50	−50	2.53E-01	2.66E-02

2 Methods

The aim of this paper is to predict the distortion of thin-walled components due to the machining-induced residual stresses. To achieve this goal, a residual stresses prediction model based on the cutting conditions and a distortion prediction model based on the predicted residual stress distribution are established. Moreover, a modification method of the predicted

Table 2 Parameters of the electro-polishing method

Chemical compositions	Methanol	200 ml
	ethylene glycol monobutyl ether	100 ml
	$HCLO_4$	20 ml
Electrolytic parameters	Voltage	20 V
	Current density	0.1–0.15 A/cm^2
	Polishing rate	20 nm/s

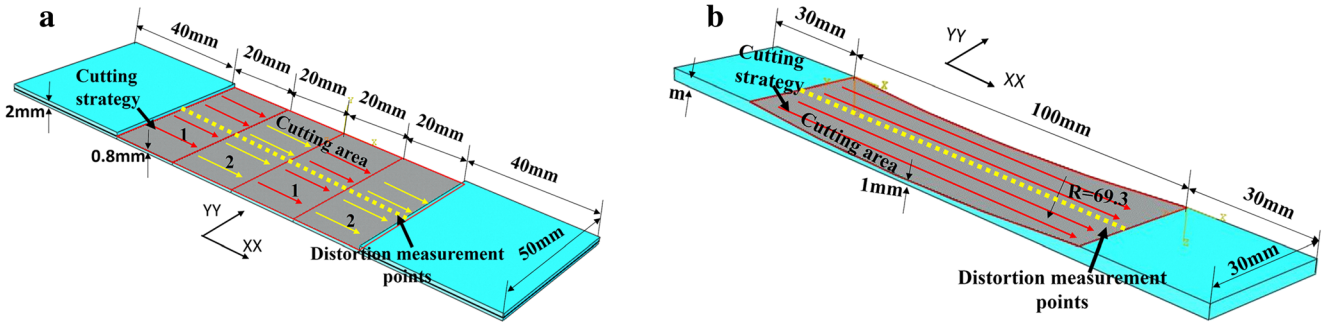

Fig. 4 Details of the experimental samples.**a** sample 1; **b** sample 2

residual stress distributions is proposed to reduce the influence of the prediction errors of residual stresses on the final distortion. The concrete realization steps of the prediction are given in Fig. 1. First, sufficient cutting experiments under different cutting conditions are conducted to establish the residual stress prediction model. Second, the cutting conditions of the experimental sample are analyzed, and the residual stress distributions are predicted for each cutting condition. It is important to note that the experimental samples are machined under several cutting conditions or are complex thin-walled parts or both. Then, standard parts which are simple thin plates are machined for modification. Each standard part corresponds to one cutting condition of the experimental sample. The distortions of standard parts are both measured and simulated. The residual stress distributions are modified according to the comparison of the distortion results. Finally, the modified residual stress distributions are applied to the experimental samples based on cutting conditions to obtain the final distortion.

Table 3 Coefficients of the fitting model

	Num	*f* mm/z	v_c m/min	*C*	*k*	*w* m^{-1}	φ Rad	R^2
σ_{xx}	1	0.04	60	1247	0.62	28.5	3.57	0.98
	2	0.08	60	1081	0.56	26.3	3.66	0.98
	3	0.06	80	419	0.62	34.8	3.15	0.89
	4	0.06	60	857	0.29	24.4	3.73	0.95
	5	0.04	80	268	0.45	42.7	3.40	0.94
	6	0.08	40	756	0.57	30.5	3.62	0.97
	7	0.04	40	805	0.69	29.6	3.51	0.97
σ_{yy}	1	0.04	60	792	0.55	43.4	3.19	0.92
	2	0.08	60	726	0.63	43.1	3.09	0.98
	3	0.06	80	620	0.95	42.7	2.75	0.87
	4	0.06	60	837	0.60	37.8	2.93	0.94
	5	0.04	80	205	0.71	67.0	1.83	0.91
	6	0.08	40	600	0.57	35.3	3.17	0.96
	7	0.04	40	483	0.54	41.9	2.99	0.86

2.1 Empirical modeling of the machining induced residual stresses

Numerical and empirical models are two main methods for predicting machining residual stresses induced by ball end milling and the empirical method has higher prediction accuracy [17]. The empirical method is chosen for residual stress prediction in this paper. The empirical model for predicting the machining-induced residual stresses includes two parts: the residual stress profile fitting model and the regression model for fitting coefficients based on cutting parameters. The residual stress profile fitting model provides the fitting function for the near surface residual stress profiles under different cutting conditions while the regression model based on cutting parameters describes the relationship between the fitting functions and the cutting parameters.

2.1.1 Residual stress profile fitting model

It is reported by researchers that the machining induced residual stress profiles usually show a similar shape: A tensile (or small compressive) peak at the surface followed by a compressive peak settling at a distance without becoming positive again, or very small positive values [18, 19]. Several typical residual stress distributions induced by milling are given in Fig. 2, in which σ_{xx} means the residual stresses in the direction parallel to feed while σ_{yy} means the residual stresses in the direction perpendicular to feed.

As can be seen in Fig. 2, the residual stress profiles show a rule of the under damped decay curve. Thus, an exponentially decaying sine function (Eq.1) which is a damped decaying function is used to represent these hook-shaped residual stress profiles.

$$\sigma(h) = Ce^{-kwh/\sqrt{1-k^2}}\sin(wh+\varphi) \quad (1)$$

where $\sigma(h)$ is the value of residual stress, h is the distance to the machined surface, C is amplitude constant, k is the decay coefficient, w is the decay frequencies, and φ is the phase angle. Particle swarm optimization (PSO) method is used to

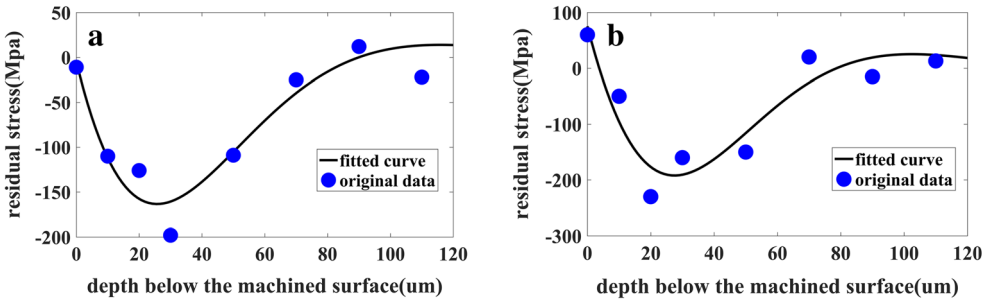

Fig. 5 Worst fits. **a** profile in XX direction; **b** profile in YY direction

find the optimal values of coefficients in the exponentially decaying sine function. The squared correlation coefficient R^2 is used to evaluate the fitting effect.

2.1.2 Prediction model of the residual stresses based on cutting parameters

Regression functions are established to describe the relationships between the coefficients of the fitting function and the cutting parameters in order to achieve predictable results. The function model shown by Eq.2 is chosen to represent the relationships.

$$y = Ax_1{}^{\alpha_{11}}\alpha_{12}{}^{x_1}x_2{}^{\alpha_{21}}\alpha_{22}{}^{x_2}\ldots x_n{}^{\alpha_{n1}}\alpha_{n2}{}^{x_n} \quad (2)$$

Where y is the value of the coefficients of fitting model, which refer to the values of C, k, w, and φ. A is amplitude constant. $x_1 \ldots x_n$ refers to different cutting parameters. $\alpha_{11} \ldots \alpha_{n1}$, $\alpha_{12} \ldots \alpha_{n2}$ are constant values. n are the number of cutting parameters being analyzed. The solution processes of regression functions are conducted with the general global optimization algorithm.

Table 4 Regression functions

Direction	Coefficients	Functions
XX	C	$2.4e^{-10}f^{-0.522}9025^{f}v_c{}^{9.206}0.837^{v_c}$
	k	$2.030f^{-0.853}166193^{f}v_c{}^{-1.417}1.021^{v_c}$
	w	$0.050f^{-0.657}13634^{f}v_c{}^{-1.119}1.027^{v_c}$
	φ	$0.202f^{0.104}0.224^{f}v_c{}^{1.123}0.978^{v_c}$
YY	C	$1214f^{1.754}(3.616e^{-9})^{f}v_c{}^{1.638}0.981^{v_c}$
	k	$21925f^{1.216}(4.421e^{-7})^{f}v_c{}^{-2.264}1.053^{v_c}$
	w	$0.026f^{-1.132}20480^{f}v_c{}^{-1.271}1.030^{v_c}$
	φ	$0.362f^{1.032}(7.90e^{-8})^{f}v_c{}^{2.133}0.956^{v_c}$

2.2 Prediction model for the distortion induced by machining residual stresses

Finite element simulation of machining distortion is performed using the commercial FEM software ABAQUS. The assumption is adopted that the workpiece has underwent stress relief treatment after rough machining and a small amount of material will be removed in the finishing stage. The effect of the bulk stresses is ignored in our analysis. The boundary conditions are set according to the experiments. The workpiece is meshed with C3D8R element. The near surface layer, 105 μm in thickness, is specially divided into seven uniform shells along the thickness direction, with each shell being 15 μm thick. The predicted milling-induced residual stress data are dispersed and the mean stress values of each shell are averaged based on the principle expressed by Eq. 3. The calculated mean stress of each shell is applied to the finite element model layer by layer to obtain the final distortion.

$$\overline{\sigma_i} = \frac{\int_{h_i}^{h_{i+1}} \sigma(h)dh}{h_{i+1} - h_i} \quad (3)$$

where $\overline{\sigma_i}$ is the mean stress of each shell, i is the number of each shell and h_i,h_{i+1} are the depth of the top and bottom edge of each shell, respectively.

2.3 Modification method of the predicted machining residual stresses

A modified method is proposed in order to reduce the prediction error of distortion caused by prediction errors of machining residual stresses. Standard parts were machined with the cutting parameters used in the machining of experimental samples. Each standard part corresponds to one cutting condition. The relationship between the machining induced residual stresses and distortion of the stand part was analyzed by simulations. Details of the standard parts used in this paper are given in Fig. 3. The cutting area is 80 mm long and 30 mm wide. The thickness of the machining area is 1 mm. The material is Inconel 718.

Different values of average residual stresses were applied to the near surface layer (105 μm in thickness) and the

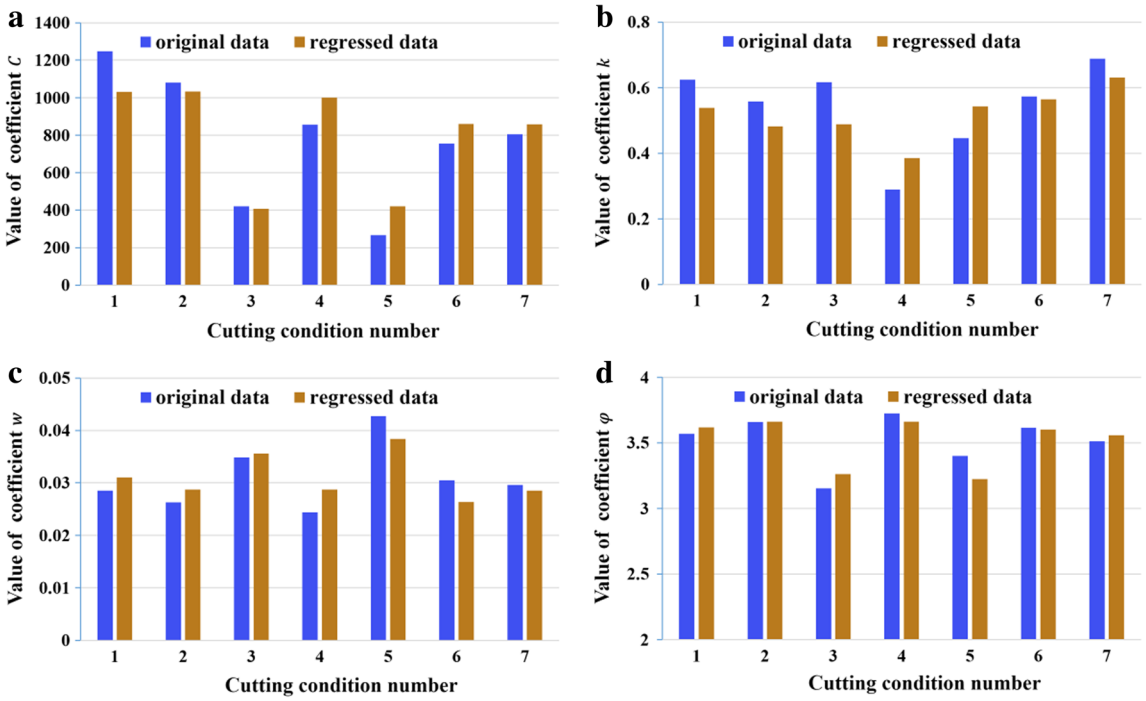

Fig. 6 Regression effects in XX direction. **a** C; **b** k; **c** w; **d** φ

distortions of the standard part were obtained in the FEM software. The results are shown in Table 1, $\overline{\sigma}_{xx}$ is the averaged machining induced residual stress in the near surface layer in the length direction (XX direction) and $\overline{\sigma}_{yy}$ is the averaged machining-induced residual stress in the near surface layer in the width direction (YY direction). In this paper, σ_{xx}means the residual stresses in the direction parallel to feed while σ_{yy} means the residual stresses in the direction perpendicular to feed. δ_{xx} is the distortion of the machined parts along the central line in the length direction while δ_{yy} is the distortion along the central line in width direction. The measurement points of distortions are also shown in Fig. 3. The negative

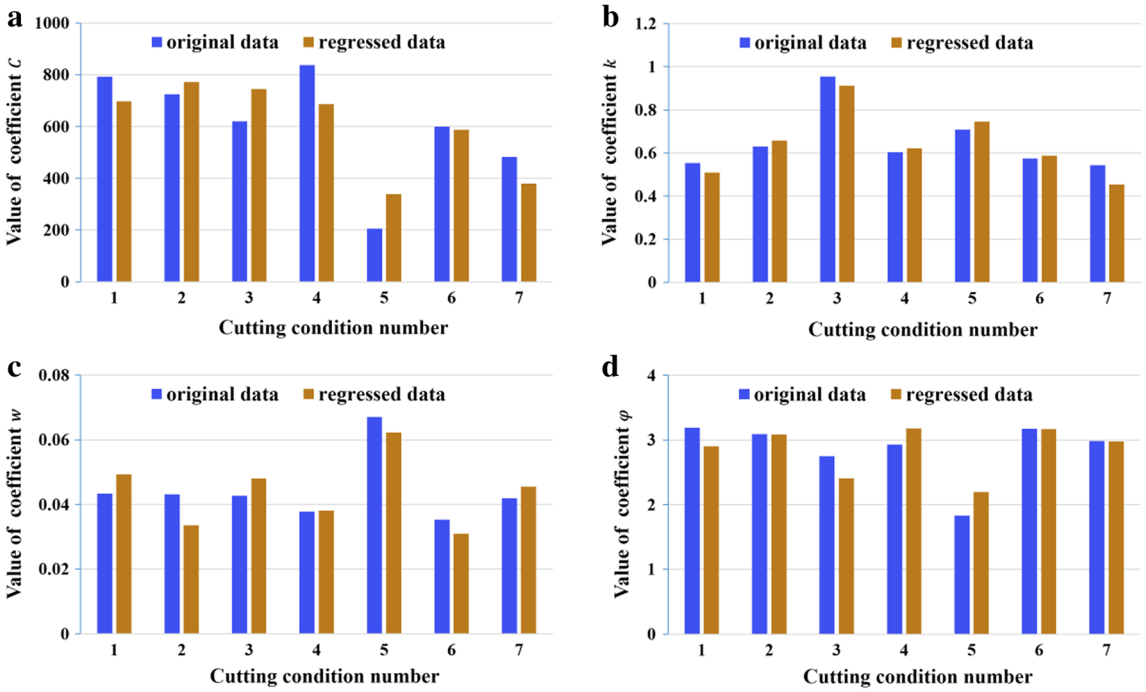

Fig. 7 Regression effects in YY direction. **a** C; **b** k; **c** w; **d** φ

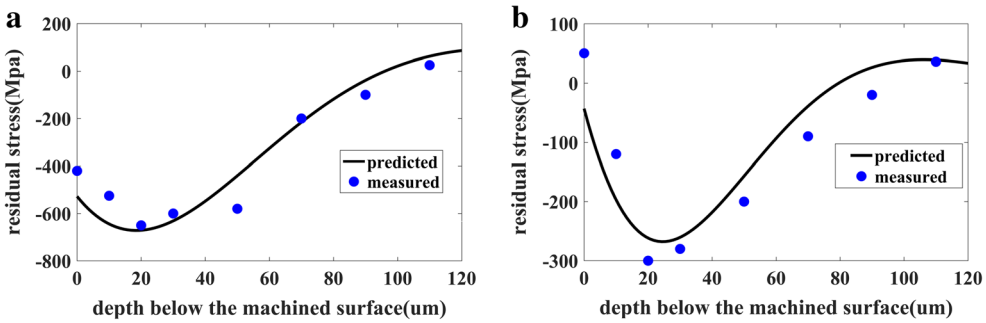

Fig. 8 Measured and predicted residual stress profiles **a** in XX direction; **b** in YY direction

values of distortion refer to concave distortion and the positive values refer to upper convex distortion.

The relationship can be obtained by regression between the residual stresses and distortions, as shown in Eq. 4 and Eq. 5.

$$\overline{\sigma}_{xx} = 0.1759 - 165.8027\delta_{xx} - 298.6101\delta_{yy} \quad R^2 = 1 \tag{4}$$

$$\overline{\sigma}_{yy} = -0.0486 - 48.9814\delta_{xx} - 1412.9702\delta_{yy} \quad R^2 = 1 \tag{5}$$

All the standard parts were machined at the corresponding cutting conditions. The distortions of the standard parts were measured and compared with the FEM simulation results. The modification factor λ will be obtained by Eq. 6 and Eq. 7.

$$\lambda_{xx} = \frac{\overline{\sigma}_{xxMea}}{\overline{\sigma}_{xxPre}} = \frac{0.1759 - 165.8027\delta_{xxMea} - 298.6101\delta_{yyMea}}{0.1759 - 165.8027\delta_{xxSim} - 298.6101\delta_{yySim}} \tag{6}$$

$$\lambda_{yy} = \frac{\overline{\sigma}_{yyMea}}{\overline{\sigma}_{yyPre}} = \frac{-0.0486 - 48.9814\delta_{xxMea} - 1412.9702\delta_{yyMea}}{-0.0486 - 48.9814\delta_{xxSim} - 1412.9702\delta_{yySim}} \tag{7}$$

Whereλ_{xx}refers to the modification factor of residual stresses in the length direction, λ_{yy}refers to the modification factor of residual stresses in the width direction. $\overline{\sigma}_{xxMea}, \overline{\sigma}_{yyMea}$ refer to the residual stress calculated by measured distortion results, $\overline{\sigma}_{xxPre}, \overline{\sigma}_{yyPre}$ refer to the residual stress calculated by simulated distortion results. $\delta_{xxMea}, \delta_{yyMea}$ refer to the measured distortion of standard parts and $\delta_{xxSim}, \delta_{yySim}$ refer to the simulated distortion of standard parts.

Finally, the residual stress profiles were modified according to Eq. 8 and Eq. 9. The distortions of the experimental sample were obtained by applying the modified residual stress profiles to the FEM model.

$$\sigma'_{xx}(h) = \lambda_{xx} C e^{-kwh/\sqrt{1-k^2}} \sin(wh + \varphi) \tag{8}$$

$$\sigma'_{yy}(h) = \lambda_{yy} C e^{-kwh/\sqrt{1-k^2}} \sin(wh + \varphi) \tag{9}$$

3 Experimental procedures

All experiments were performed with down milling operation by a CNC machine (YH V850 machine center with a SINUMERIK 840D system). The workpiece material used was Inconel 718. The solid cemented carbide ball end milling cutters (K44, Germany) were used throughout the experiments. The cutter diameter was 10 mm. The helix angle was 40°. The rake angle was 5°. The radius of the cutting edge was 0.04 mm. All experiments were performed with coolant.

In the residual stresses measurement tests, the workpiece material was prepared in 300 × 200 × 20 mm blocks. The feedrate and the cutting speed were varied for residual stresses analysis. Three levels of feedrate (0.04, 0.06, 0.08 mm/Z) and cutting speed (40, 60, 80 m/min) were employed. A 20 mm × 20 mm plane was finish machined with a new cutter for each cutting condition to obtain machined surface samples. The state of residual stresses in the machined surface was measured using X-ray diffraction. Measurements were performed on Proto LXRD X-ray stress analyzer using Mn Ka radiation at 30 kV (15 mA) to acquire the diffraction peak at a Bragg's angle.

Table 5 The predicted stresses under two cutting conditions

	v_c=40 m/min, f=0.05 mm/z	v_c=60 m/min, f=0.05 mm/z
σ_{xx}	$\sigma(h) = 822e^{-0.0196h}\sin(0.027h + 3.55)$	$\sigma(h) = 974e^{-0.0169h}\sin(0.029h + 3.59)$
σ_{yy}	$\sigma(h) = 469e^{-0.0228h}\sin(0.038h + 3.14)$	$\sigma(h) = 621e^{-0.0290h}\sin(0.041h + 3.03)$

Table 6 The modified residual stresses under two cutting conditions

	v_c=40 m/min, f=0.05 mm/z	v_c=60 m/min, f=0.05 mm/z
σ_{xx}	$\sigma(h) = 711e^{-0.0196h}\sin(0.027h + 3.55)$	$\sigma(h) = 793e^{-0.0169h}\sin(0.029h + 3.59)$
σ_{yy}	$\sigma(h) = 387e^{-0.0228h}\sin(0.038h + 3.14)$	$\sigma(h) = 520e^{-0.0290h}\sin(0.041h + 3.03)$

Material removal by electro-polishing was applied. Parameters of the electro-polishing method are shown in Table 2. This process is repeated seven times to obtain the depth of 105 μm. For each layer, residual stresses were also measured in two directions: perpendicular (YY direction) and parallel to feed (XX direction), respectively.

Two experimental samples were analyzed in this paper. One is a thin walled plate machined with two cutting conditions and the other one is a curved part machined with one cutting condition. The details of the two experimental samples are shown in Fig. 4. Sample 1 was machined under two cutting condition while area 1 was machined at v_c=60 m/min, f=0.05 mm/z and area 2 was machined at v_c=40 m/min, f=0.05 mm/z. Sample 2 was machined at v_c=60 m/min, f=0.05 mm/z.

In order to assess the distortion level, the distortions of the machined parts were measured along the central line in the length direction by an on-machine measurement equipment. In the distortion measurement tests, the workpieces were prepared in 160 × 50 × 2 mm blocks for sample 1 and 160 × 30 × 3 mm blocks for sample 2. The standard parts for modification were prepared in 160 × 30 × 2 mm blocks. All the workpieces were placed on the milling table with two ends clamped in the fixture to eliminate the influence of elastic deformation caused by cutting forces. The cutting strategies of the workpieces were given in Figs. 3 and 4. Only one cutting condition of the experimental samples was adopted by each standard part.

4 Results and discussion

4.1 Results of the prediction model of the residual stress profiles

The empirical models for fitting the residual stresses were established based on the measured results. Both the results in XX direction and YY direction were modeled for further discussion. Coefficients of the fitting models are shown in Table 3. It can be observed that the R^2 values of the fitting model in XX direction changed from 0.89 to 0.98 and the R^2 values of the fitting model in YY direction changed from 0.86 to 0.98, which means that the fitting model fits the measured results well.

The worst fits in XX direction and YY direction are shown in Fig. 5, respectively. It can be seen that even the worst ones still have a good fitness.

The regress parameters were calculated, regression functions of the coefficients in the exponentially decaying sine function are given in Table 4

The regression effects are shown in Figs. 6 and 7. The corresponding titles of X axis are the cutting condition numbers which refers to the cutting conditions number in Table 3. The Y coordinates represent the values of coefficients of the fitting function of residual stress profiles. It can be seen that the correlated results are satisfactory.

Figure 8 gives the measured and the predicted residual stress profiles at v_c=50 m/min, f=0.05 mm/z. As shown in Fig. 8, the predicted stress profiles are found to be in good

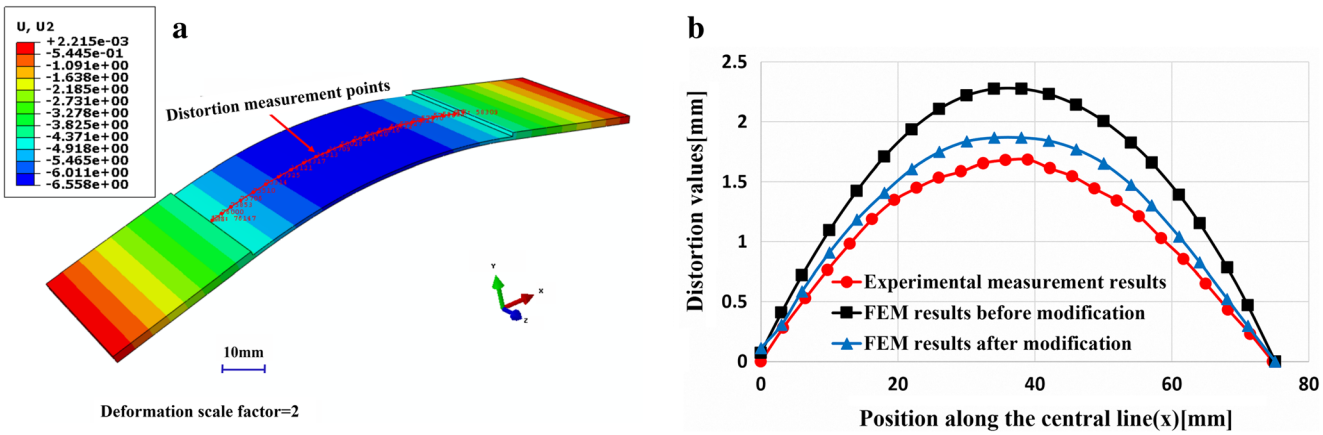

Fig. 9 Distortions of sample 1. **a** Distortion nephogram after modification, **b** Distortions along the central line(XX)

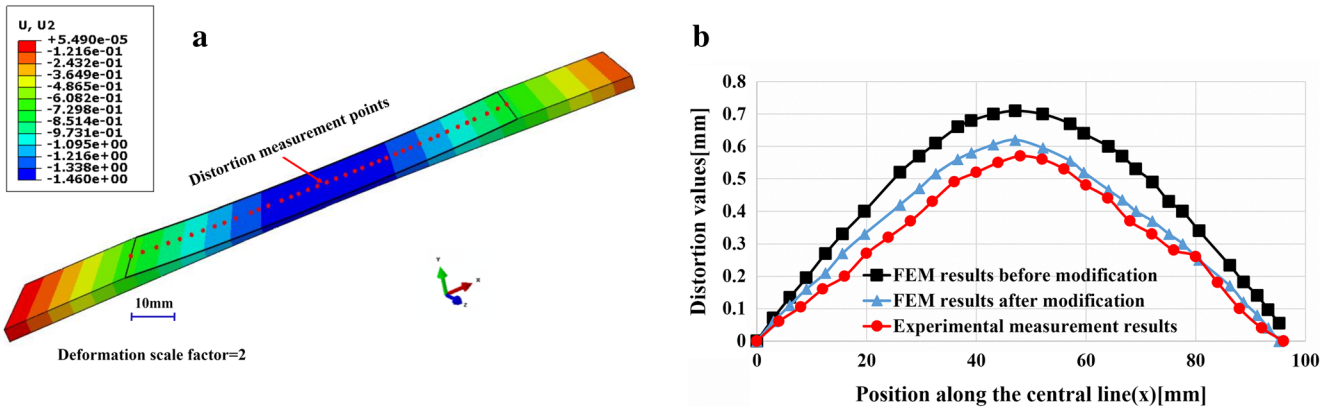

Fig. 10 Distortions of sample 2. **a** Distortion nephogram after modification, **b** Distortions along the central line(XX)

agreement with the measured ones. This validation shows that it is possible to predict the residual stress profile with good accuracy using the proposed predicting model.

4.2 Results of the prediction model of distortion

The residual stress profiles under the two cutting conditions used in the machining of experimental samples were predicted using the residual stress predicting model proposed in this paper. The predicted residual stress profiles are listed in Table 5.

Obvious distortions were observed on the experimental parts. As the cutting processes mainly induce compressive residual stresses, all the parts show upper convex deformations. Distortion measurements were conducted along the central line in the length direction. The measured distortion of the two standard parts were 0.724 mm at v_c=40 m/min, f=0.05 mm/z and 0.852 mm at v_c=60 m/min, f=0.05 mm/z in the XX direction, while the FEM results were 0.832 mm at v_c=40 m/min, f=0.05 mm/z and 1.034 mm at v_c=60 m/min, f=0.05 mm/z in the XX direction. The measured distortion of the two standard parts were 0.008 mm at v_c=40 m/min, f=0.05 mm/z and 0.013 mm at v_c=60 m/min, f=0.05 mm/z in the YY direction, while the FEM results were 0.012 mm at v_c=40 m/min, f=0.05 mm/z and 0.015 mm at v_c=60 m/min, f=0.05 mm/z in the YY direction. Then, the modification factors $\lambda_{xx40} = 0.865$, $\lambda_{yy40} = 0.814$, $\lambda_{xx60} = 0.825$, $\lambda_{yy60} = 0.837$were obtained according to Eq. 6 and Eq. 7. The modified residual stress profiles are shown in Table 6.

By applying the modified residual stresses to the FEM model, the distortion of the experimental parts was obtained. Both experimental parts show convex distortions.

As shown in Fig. 9, the maximum measured distortion value of the cutting area of the experimental sample 1 was 1.68 mm. The predicted result before modification was 2.28 mm while the result after modification was 1.87 mm. The predictive error is reduced from 35 to 11%.

As shown in Fig. 10, the maximum measured distortion value of the cutting area of the experimental sample 2 was 0.57 mm. The predicted result before modification was 0.71 mm while the result after modification was 0.62 mm. The predictive error is reduced from 25 to 9%.

It can be seen in Figs. 9 and 10 that the prediction accuracy of the experimental samples is significantly improved after modification by simple standard parts, which illustrates the effectiveness of the proposed method. However, the simulated results are still bigger than those of the experimental results in both samples. This is due to the influences of tool wear. Tool wear is more serious in the machining of experimental samples due to the larger cutting areas. Tool wear results in a dramatic increase in cutting temperature. As the thermal stresses mainly induce tensile stresses, the peak compressive stress values in the experiments decrease, which results in the decrease of distortions.

5 Conclusion

The objective of this study is to propose a method of predicting distortion of thin-walled parts induced by machining residual stresses. An empirical model for predicting machining induced residual stresses under different cutting conditions was built by conducting sufficient cutting experiments. A good agreement was obtained between the predictive results and experimental data. A FEM model for distortion predicting was used and a modification method was proposed. Standard parts which are simple thin plates were machined firstly to modify the residual stresses which were applied to the FEM model of complex experimental samples. Two experimental samples were used to validate the predicting method. The predictive error of sample 1 is reduced from 35 to 11% after modification. The predictive error of sample 2 is reduced from 25 to 9% after modification. The results show that the method can predict the distortion caused by machining induced residual stresses more accurately.

Acknowledgements This study was supported by the National Natural Science Foundation, China (No. 51475382).

References

1. Bowden DM, Halley JE (2000) Aluminum reliability improvement program-final report. The Boeing Company, Chicago
2. Ma Y, Feng P, Zhang J, Wu Z, Yu D (2016) Prediction of surface residual stress after end milling based on cutting force and temperature. J Mater Process Technol 235:41–48. https://doi.org/10.1016/j.jmatprotec.2016.04.002
3. Sadat AB, Reddy MY (1992) Surface integrity of Inconel 718 nickel base superalloy using controlled and natural contact length tools, Part 1. Lubricated, Exp Mech 282–288
4. Sadat AB, Reddy MY (1993) Surface integrity of Inconel 718 nickel base superalloy using controlled and natural contact length tools, Part 2. Unlubricated, Exp. Mech 343–348
5. Schlauer C, Peng RL, Oden M (2002) Residual stresses in a nickel-based superalloy introduced by turning. Mater Sci Forums 404-407: 173–178. https://doi.org/10.4028/www.scientific.net/MSF.404-407.173
6. Outeiro JC, Dias AM, Jawahir IS (2006) On the effects of residual stresses induced by coated and uncoated cutting tools with finite edge radii in turning operations. CIRP Ann Manuf Technol 55(1): 111–116. https://doi.org/10.1016/S0007-8506(07)60378-3
7. Huang X, Sun J, Li J (2015) Finite element simulation and experimental investigation on the residual stress-related monolithic component deformation. Int J Adv Manuf Technol 77(5-8):1035–1041. https://doi.org/10.1007/s00170-014-6533-9
8. Yang Y, Li M, Li K (2014) Comparison and analysis of main effect elements of machining distortion for aluminum alloy and titanium alloy aircraft monolithic component. Int J Adv Manuf Technol 70(9-12):1803–1811. https://doi.org/10.1007/s00170-013-5431-x
9. Young KA (2005) Machining-induced residual stress and distortion of thin parts. PhD, Washington University, USA
10. Marusich TD, Usui S, Terauds KJ (2008) Finite element modelling of part distortion. In: proceedings of the 2nd international conference in distortion Engineering 133–142
11. Zhang Z, Li L, Yang Y, He N, Zhao W (2014) Machining distortion minimization for the manufacturing of aeronautical structure. Int J Adv Manuf Technol 73(9-12):1765–1773. https://doi.org/10.1007/s00170-014-5994-1
12. Brinksmeier E, Solter J (2009) Prediction of shape deviations in machining. CIRP Annal 58(1):507–510. https://doi.org/10.1016/j.cirp.2009.03.123
13. Cerutti X, Arsene S, Mocellin K (2016) Prediction of machining quality due to the initial residual stress redistribution of aerospace structural parts made of low-density aluminium alloy rolled plates. Int J Mater Form 9(5):677–690. https://doi.org/10.1007/s12289-015-1254-7
14. Cerutti X, Mocellin K (2016) Influence of the machining sequence on the residual stress redistribution and machining quality: analysis and improvement using numerical simulations. Int J Adv Manuf Technol 83(1-4):489–503. https://doi.org/10.1007/s00170-015-7521-4
15. Fergani O, Lazoglu I, Mkaddem A, Mansori ME, Liang SY (2014) Analytical modeling of residual stress and the induced deflection of a milled thin plate. Int J Adv Manuf Technol 75(1-4):455–463. https://doi.org/10.1007/s00170-014-6146-3
16. Masoudi S, Amini S, Saeidi E, Eslami-Chalander H (2015) Effect of machining-induced residual stress on the distortion of thin-walled parts. Int J Adv Manuf Technol 76(1-4):597–608. https://doi.org/10.1007/s00170-014-6281-x
17. Wang J, Zhang D, Wu B, Luo M (2017) Numerical and empirical modelling of machining-induced residual stresses in ball end milling of Inconel 718. Procedia CIRP 58:7–12. https://doi.org/10.1016/j.procir.2017.03.177
18. Ulutan D, Arisoy YM, Özel T, Mears L (2014) Empirical modeling of residual stress profile in machining nickel based superalloys using the exponentially decaying cosine function. Procedia CIRP 13:365–370. https://doi.org/10.1016/j.procir.2014.04.062
19. Yang D, Liu Z, Ren X, Zhuang P (2016) Hybrid modeling with finite element and statistical methods for residual stress prediction in peripheral milling of titanium alloy. Int J Mech Sci 108-109:29–38. https://doi.org/10.1016/j.ijmecsci.2016.01.027
20. Wang J, Zhang D, Wu B, Luo M (2017) Residual stresses analysis in ball end milling of nickel-based Superalloy Inconel 718. Mater Res https://doi.org/10.1590/1980-5373-mr-2017-0561